

# Simulations of Ultrasonographic Periodontal Probe Using the Finite Integration Technique

Kevin Rudd, Crystal Bertoncini and Mark Hinders\*

*Applied Science Department of the College of William and Mary in Virginia, NDE Lab @ 116 Jamestown Road, Williamsburg, VA 23187-8795, USA*

**Abstract:** Periodontal disease is one of the most pervasive dental diseases in older adults. It involves the loss of connective tissue attachment with subsequent destruction of tooth-supporting bone, leading to loss of teeth. Periodontal pocket depth is currently measured with an invasive manual probe, but adapting diagnostic ultrasound to this purpose can avoid the pain and inaccuracy inherent in manual probing. In this paper, 3D simulations of ultrasonic periodontal probe measurements are described, using a parallel finite integration technique which is adaptable enough to create realistic anatomical geometries. The outputs of the simulation include 3D pressure values distributed throughout the periodontal anatomy, 2D vertical cross sections of the acoustic pressure waves, and the pressure across the face of the transducer which is used to synthesize the ultrasonic echo. Experimental comparison with a simple phantom is also shown. Lastly, the energy values for different simulations are calculated from the 3D pressure values to describe the amount of energy reaching different zones, especially the junctional epithelium. The simulations as well as the energy studies show that only a small portion of the ultrasonic energy is reaching the junctional epithelium, and so sophisticated mathematical techniques are required to ultrasonically measure pocket depth.

## 1. INTRODUCTION

Periodontal disease is an inflammatory process of the soft tissues supporting teeth due to bacterial accumulations below the gum line, and if untreated can lead to a progressive loss of attachment between the tooth and the underlying alveolar bone eventually leading to tooth loss [1]. A site-specific disease, it is characterized by localized periodontal pockets, which form between the tooth and the supporting tissue [1, 2]. Half of the adult population in the United States has mild inflammation, called gingivitis, and about 30% of the population has the more serious periodontal disease defined as having three or more periodontal pockets with depths of 4 mm or more [3-7]. Between 5% and 15% of adults with periodontal disease have advanced forms with pocket depths measuring 6mm or more [8]. Periodontal disease has been associated with diabetes, stroke, and adverse pregnancy conditions [9-11] as well as with cardiovascular disease [12-14].

Periodontal disease is diagnosed via manual probing [15] wherein a clinician locates and then determines the depth of the periodontal pocket by inserting a thin metal probe directly into the pocket. Ridges or markings on the probe indicate the depth of the pocket relative to the gum line. Manual probing has been shown to be unreliable [16-22] and it can be painful. Studies with controlled-force probes have shown success in reducing operator-related error and subjectivity inherent in manual probing [23-26] but these probes do not

account for anatomic and inflammatory factors that can affect measurement accuracy [27, 28]. Non-invasive techniques based on ultrasound may be able to diagnose periodontal disease more reliably than manual techniques while being more comfortable to the patient.

### 1.1. The Ultrasonic Periodontal Probe

Over the past four decades, many researchers have explored the use of diagnostic ultrasound to image the periodontal region [29-38]. In 1998, Loker and Hagenbuch developed a prototype of an ultrasonic device to measure the depth of the periodontal pocket [39]. Their device used a solid taper-delay line to couple the ultrasound into the tissue at approximately the same location and orientation as manual probing [40]. Results from a pilot clinical trial showed that correlation between measurements taken by manual probing and with their ultrasonic device were "not particularly good".

Also in 1998, Companion and Hinders [41, 42] first reported results of an ultrasonic periodontal probe that had been under development at NASA Langley for several years [43, 44]. This ultrasonic periodontal probe [45-49] uses a hollow tapered tip that is filled with water for coupling of the ultrasonic beam into the tissues as shown in Fig. (1). The internal shape of the hollow probe tip has been optimized via a combination of computer simulations and systematic experiments, and a sequence of increasingly more practical clinical prototypes were developed and used in several pilot studies comparing ultrasonic to calibrated-manual and controlled-force probing. Pictures of the latest generation of the ultrasonic periodontal probe including the water flow system, ultrasonic probe, and the data acquisition system is shown in Figs. (2) and (3). A critical development was the

\*Address correspondence to this author at the Applied Science Department of the College of William and Mary in Virginia, NDE Lab @ 116 Jamestown Road, Williamsburg, VA 23187-8795, USA; E-mail: mark.hinders@gmail.com

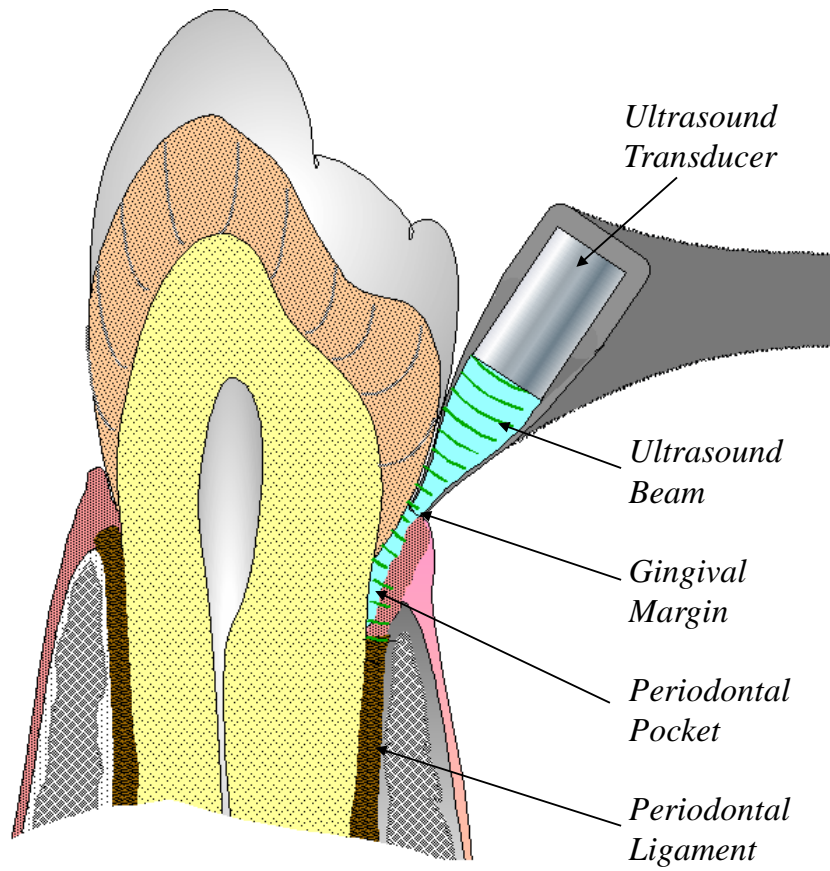


**Fig. (1).** Diagram of the ultrasonic periodontal probe and the major tissue structures of the periodontal region.



**Fig. (2).** Picture of the latest generation of the ultrasonographic periodontal probe system.

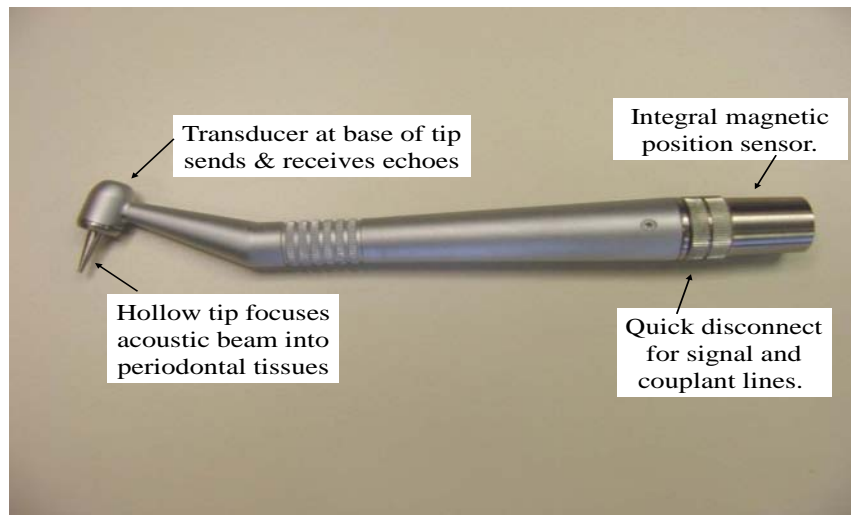


Fig. (3). Close-up picture of the ultrasonographic periodontal probe hand piece.

recognition of the need for artificial intelligence algorithms to automatically identify the very subtle echo-waveform features corresponding to the anatomy of interest. The wavelet fingerprint technique of Hou and Hinders [50-55] was adapted for this purpose and shows promise.

In this paper, we use the three-dimensional parallel acoustic finite integration technique (3DPAFIT) to simulate the ultrasound propagation in the tip and the intricate geometries periodontal tissues. These simulations provide valuable insight into the complex underlying physics of the ultrasound propagation and interaction in the soft tissues. Software was developed to automatically define the 2D and 3D geometry of the tip and the periodontal tissue structures and allow for easy modifications of these geometries. Many simulations were then completed to provide systematic data sets to assist in the development of automated software algorithms for determining the periodontal pocket depth under a variety of conditions.

**2. ACOUSTIC SIMULATIONS OF THE ULTRASONIC PERIODONTAL PROBE**

A set of software tools were developed to simulate the 3D acoustic propagation and interaction in the tip and the periodontal tissues. These automatically create the 3D geometries of interest, perform acoustic simulations on a parallel super-computer, and then process and visualize the results. The pre-processing and post-processing, including visualizations, are performed on a single desktop computer using the MATLAB programming environment while the simulations themselves are performed on William and Mary’s high performance computational cluster, SciClone<sup>1</sup>. A flow chart of the entire process is shown in Fig. (4).

First, a software system was developed to automatically create the 2D periodontal geometry using a small number of parameters which define the scenario the user wants to simu-

late. Most of the important features of the model are parameterized so that they can be changed without having to modify the simulation software. These include the geometry of the tissue structures, material parameters, the depth of the periodontal pocket, and the curvature of the tooth and tissue structure. The ultrasonic tip is also parameterized so that its shape, the angle in which it sits on top of the periodontal pocket, and the size and frequency of the transducer can be easily changed. Once these parameters are set, the MATLAB software automatically creates the appropriate 2D models which ultimately define the 3D geometry. Then, a set of input files are created that define all the simulation parameters and geometries for the 3D acoustic simulation code.

These input files are then moved to the SciClone where the 3D parallel acoustic simulations are performed. As the simulation runs, the simulation software computes and records a variety of simulation values such as acoustic pressure inside the tissue. The output files include sets of 2D pressure slices which show the acoustic wave propagation and typical A-line data that is recorded across the front of the transducer face. More details of the software components and the periodontal and tip geometries are discussed in the following sections.

**3. TWO-DIMENSIONAL PERIODONTAL TISSUE AND TIP GEOMETRY**

The geometry of the periodontal pocket and surrounding tissues is complex, with the shape and material properties of the tooth and tissues varying from tooth to tooth and from patient to patient. We have created a 2D geometry that is based on several sources including histological cross-sections and diagrams from leading periodontal disease textbooks, as shown in Fig. (5) [56-59].

A 2D model of the periodontal pocket and surrounding tissue is shown in Fig. (6). It includes the major anatomical features that are important to periodontal disease development and the ultrasound propagation. The model includes the hard tissues of the dentin, tooth enamel, and alveolar bone. It

<sup>1</sup> Information about William and Mary’s computational science cluster, SciClone, can be found at <http://www.compsci.wm.edu/SciClone/>. SciClone is funded by grants from Sun Microsystems, the National Science Foundation, and Virginia’s Commonwealth Technology Research Fund.

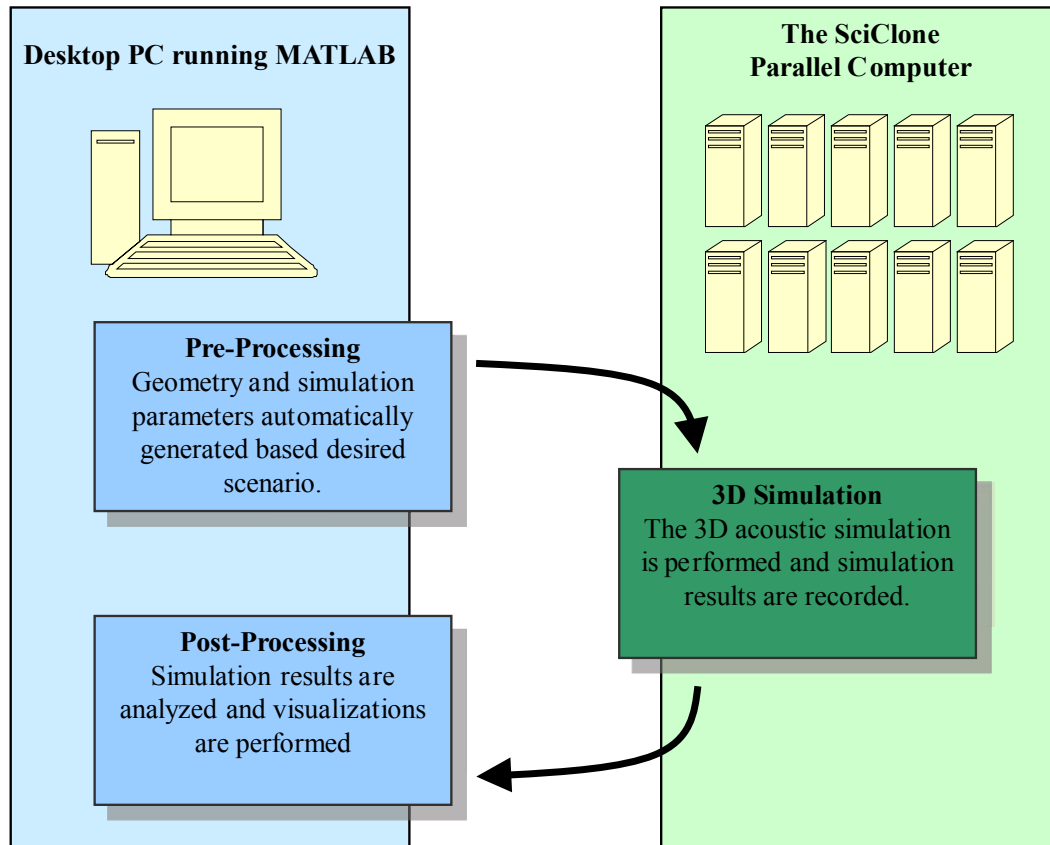


**Fig. (4).** Chart showing the flow of data from the major software components for simulating 3D acoustic waves for the ultrasonic periodontal probe.

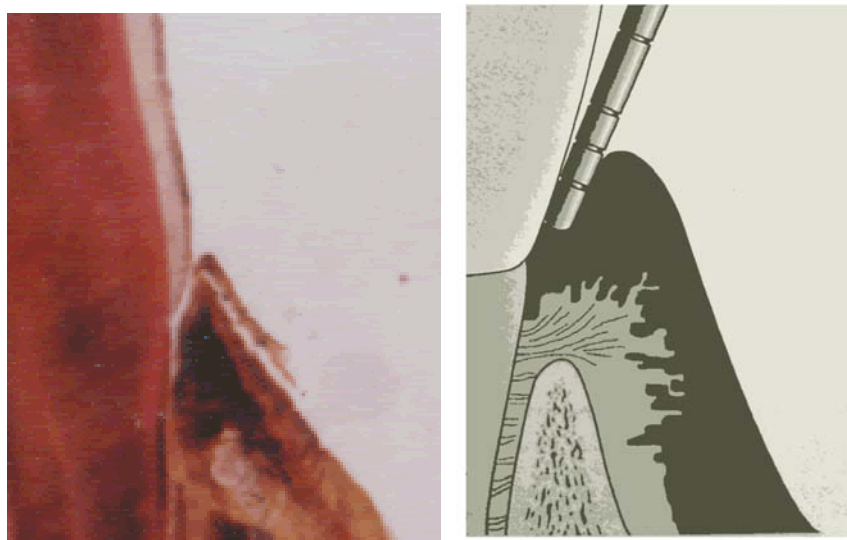


**Fig. (5).** Anatomical cross-section and a diagram of the periodontal pocket with the surrounding tissues that were used to create the 2D periodontal model.

also includes the soft tissues of the mucogingival which makes up most of the major soft tissue at the base of the tooth. The junctional epithelium (JE) is located at the base of the periodontal pocket.

The 2D model maps the geometry of the different tissue structures. The 2D model is adaptive instead of a static 2D image. The accuracy of the model can be continually improved with advice from clinicians and experts in periodon-

tics. The adaptive model of the tissue structure allows for the systematic simulations of ultrasound interactions with a broad range of geometries and pocket depths. In addition, the resolution of the 2D model can be adjusted to match the resolution of the simulation. For example, a 5 MHz simulation needs a model that is 5 times higher in resolution than a 1 MHz simulation. To perform these changes on a static image would be difficult to accomplish in a timely manner. The details of the adaptable 2D model of the periodontal tissue structures are found in the following section.

**3.1. Adaptable 2D Periodontal Tissue Model**

A software system was developed so that the entire 2D model is defined by a small set of points that indicate the boundaries between the different tissue structures. Fig. (6) shows the 2D model with a set of green points on the tissue boundaries. Once the resolution of the simulation space is determined, the rest of the boundaries are found using a cubic-spline interpolation between the major points. For example, the position, size, and shape of the alveolar bone are determined by only 5 points. The entire geometry of the model can be modified by simply moving the locations of these points or adding new ones. Once the boundaries are defined, the material parameters are filled in starting at the location of the red/blue dots.

**3.2. Adding the Periodontal Pocket**

Once the major geometry is established, the periodontal pocket is created automatically by specifying the depth of the pocket. For simplicity, the depth of the periodontal pocket is defined as the vertical distance from the top of the gum to the location of the junction between the gum and the tooth. The junctional epithelium (JE) is then positioned in the bottom of the pocket with a vertical height of 1.5 mm (this can be changed). Then the pocket is completely filled with water, which is not shown in most of the figures. Fig. (7) shows the 2D model with the periodontal pocket depth of 2 mm, 6 mm, and 10 mm.

**3.3. Two Dimensional Tip Construction and Placement**

Like the periodontal pocket, the tip of the ultrasonic probe is modeled using a 2D cross section. Previous work suggested that a tip with linear sloped walls would be the most effective shape to deliver the ultrasound energy into the periodontal pocket [48]. A 2D model of a linear tip is shown in Fig. (8). It is parameterized such that one can easily change the dimensions of the tip. These dimensions include base radius, transducer radius, wall thickness, length, and tip radius. Additional tip shapes can be modeled by specifying their cross sectional shape.

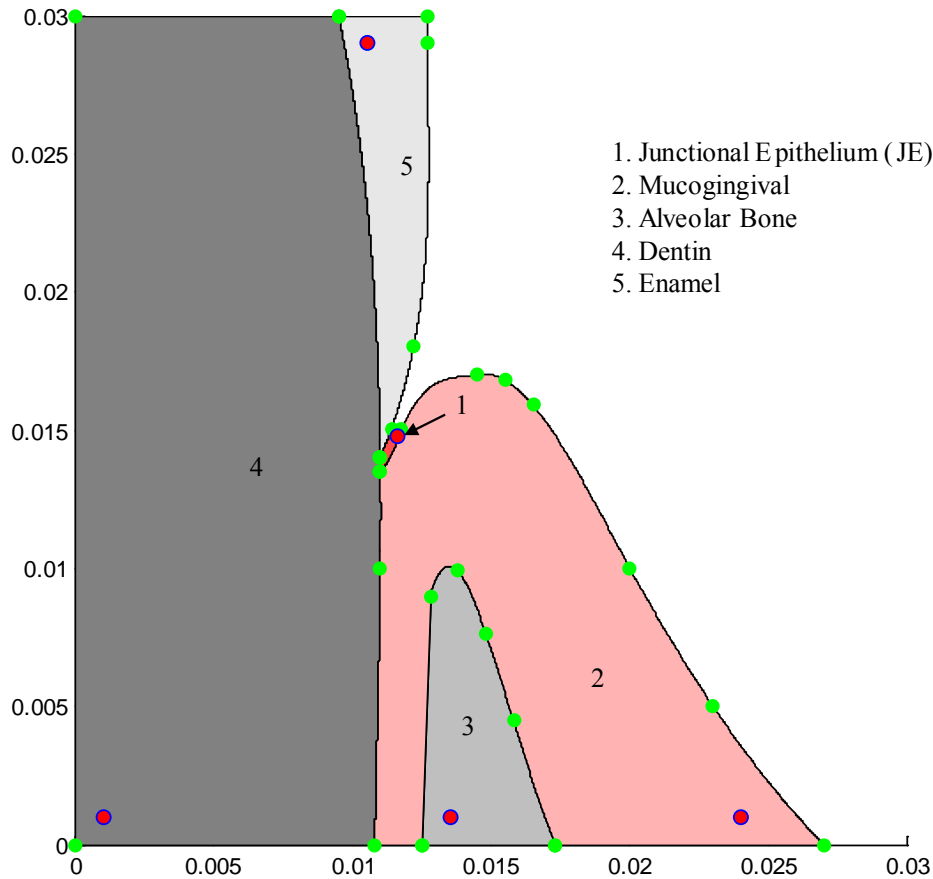


**Fig. (6).** 2D slice of the 3D periodontal model. The units of the x and y-axis of this 2D slice are in meters and correspond to the z and r-axis of a cylinder, respectively. This 2D slice is swept around the z-axis to create the 3D simulation. The 2D geometry of the periodontal tissue structures is defined by small set of points (shown in green), which indicate the boundaries between the different tissues. The entire geometry can be changed by moving these points or adding new ones.

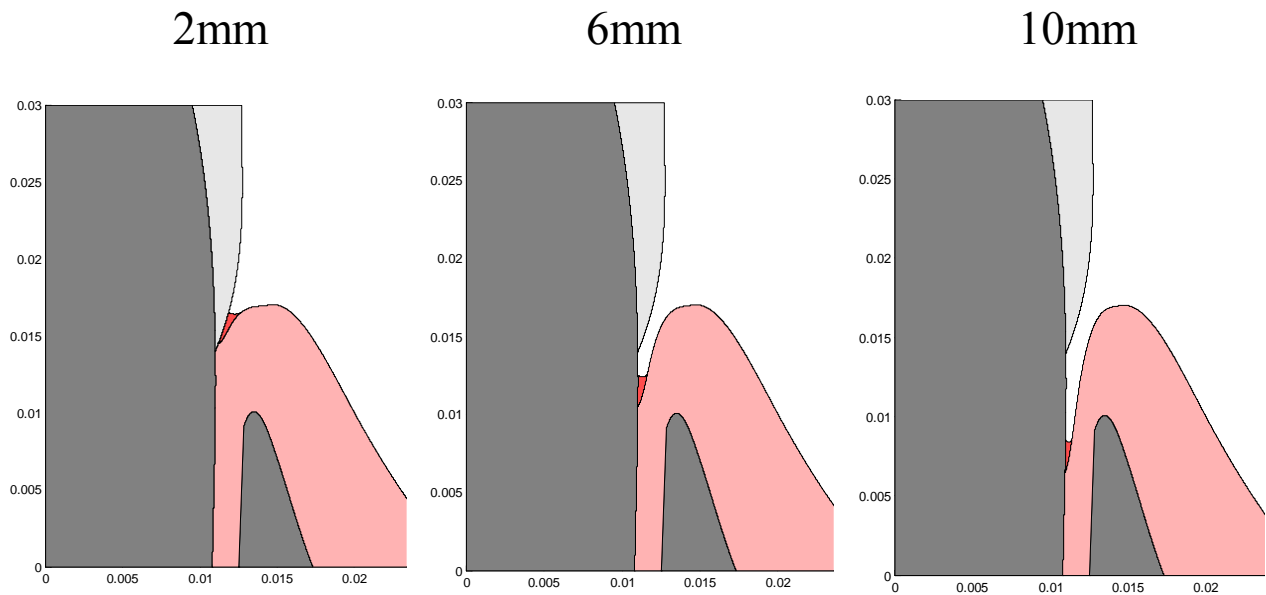


Fig. (7). The 2D periodontal model is shown for three different pocket depths.

Once the shape of the tip is defined, it is placed into position at the top of the periodontal pocket. The angle of the tip with respect to the tissue geometry is also parameterized so that it can be easily changed. The placement of the tip is completely automated. Fig. (9) shows the tip of the periodontal ultrasound probe at 65°, 50°, and 30°.

**4. THREE DIMENSIONAL PERIODONTAL POCKET AND ULTRASONIC TIP GEOMETRY**

Once the 2D geometries are defined, the 3D geometries are created by rotating or sweeping the 2D models. The 3D tip is created by rotating the 2D tip geometry 360° about its central axis. The 3D periodontal geometry is created by sweeping the 2D periodontal pocket model along the z-axis to create a curved tooth and tissue structure. An example 3D geometry with the 3D tip in place is shown in Fig. (10a). A close-up of the tip on top of the periodontal pocket is shown in Fig. (10b), where the transducer at the base of the 3D tip

is displayed in green and the water is not shown for clarity. The radius of curvature is parameterized so that tooth structures of different curvatures can be simulated.

**5. EXAMPLE SIMULATION OUTPUT AND VISUALIZATION**

Once the 3D geometries and simulation parameters are determined, a set of input files are created and passed to the 3DPFIT code which runs on a parallel super computer (The SciClone). Currently, the simulation software creates three different types of output or simulation results for the ultrasonic periodontal probe simulations.

The first is a series of vertical 2D slices through the center of the simulation space. These slices show the propagation of the acoustic waves starting from the transducer and propagating into the periodontal pocket and surrounding tissues. Fig. (11) shows a series of these snapshots for a simulation where the periodontal pocket depth is approxi-

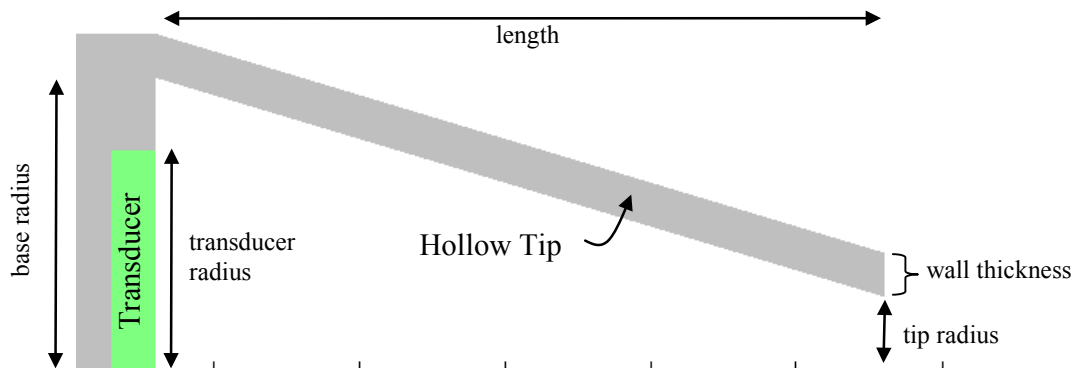


Fig. (8). A linear tip and its parameterized dimensions.

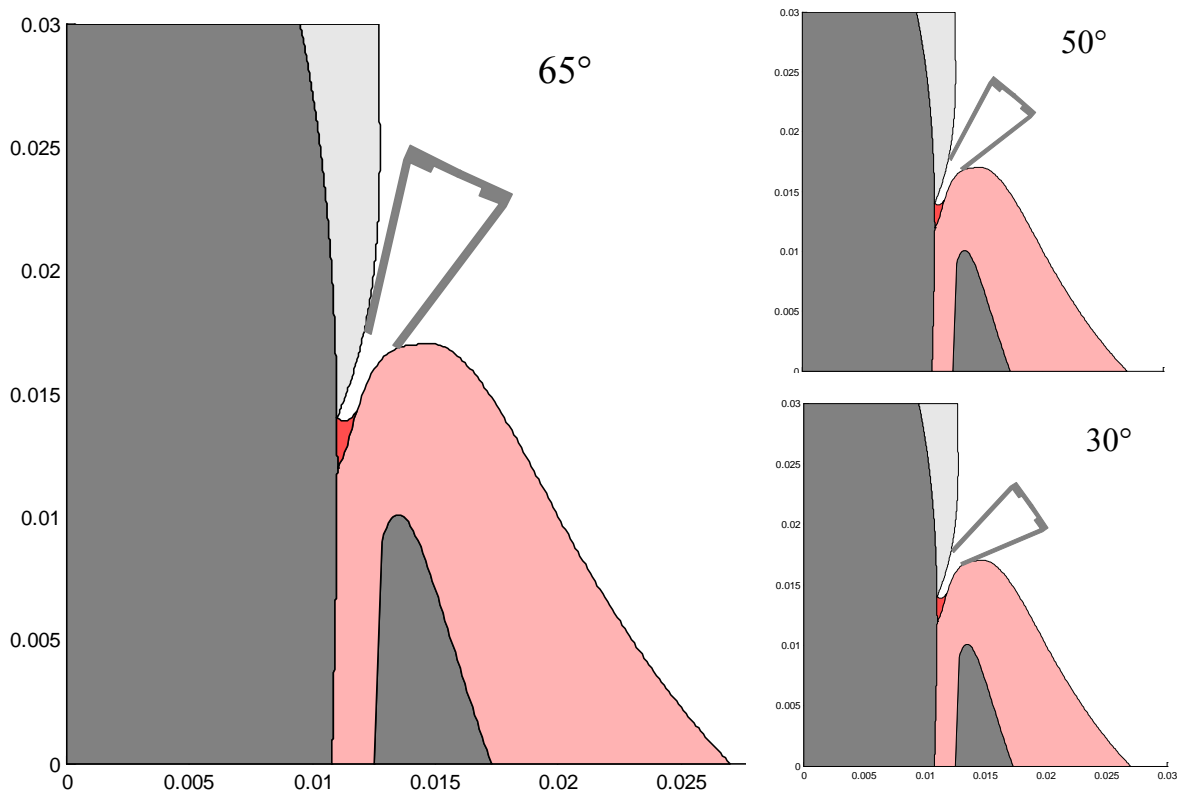


Fig. (9). The 2D periodontal model with the linear tip placed at three different angles. Once the periodontal and tip geometries are defined, the placement of the tip is done automatically.

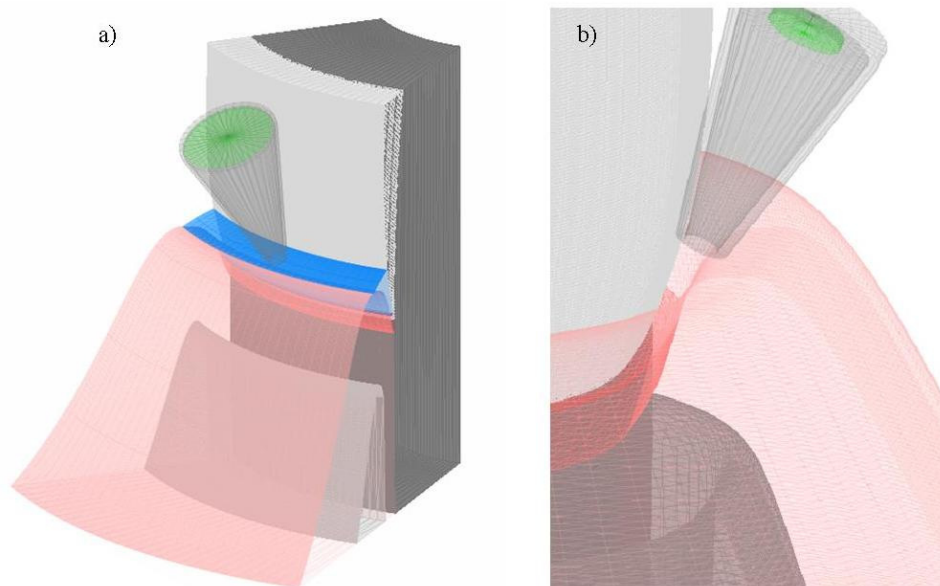
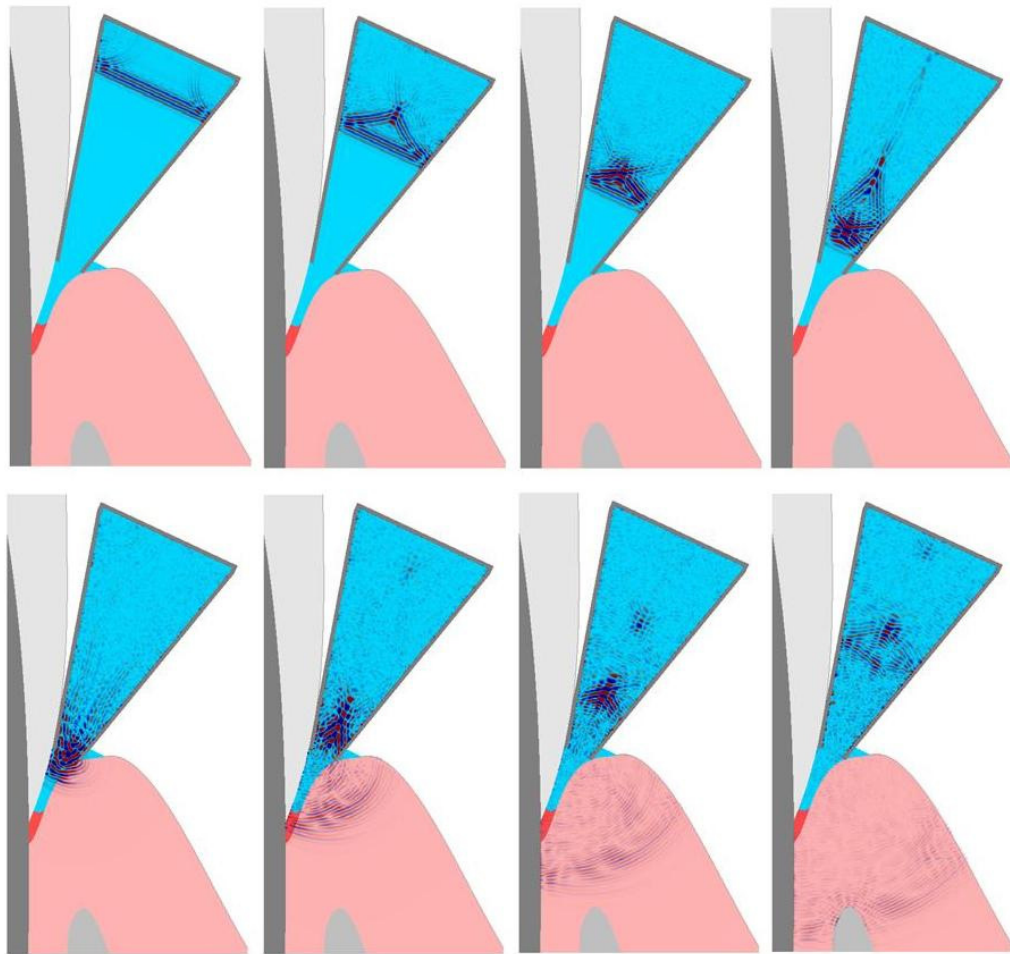


Fig. (10). (a) shows the 3D periodontal simulation geometry, while (b) shows a close-up of the tip placement without the water shown. The vertical axis here still corresponds to the z-axis from Fig. (6). The transducer at the base of the 3D tip is shown in green.

mately 2.5 mm. A movie of the 2D snapshots is also included in the supplementary material.

In addition to these 2D slices, the value of the pressure waves over the entire 3D simulation space is accumulated.

This 3D volume can be sliced to illustrate the acoustic energy distribution inside the tissue. Fig. (12) shows several horizontal slices through the volume to at three different depths below the tip. The brightness and color of these plots



**Fig. (11).** The 2D periodontal model with the linear tip placed at three different angles. Once the periodontal and tip geometries are defined, the placement of the tip is done automatically.

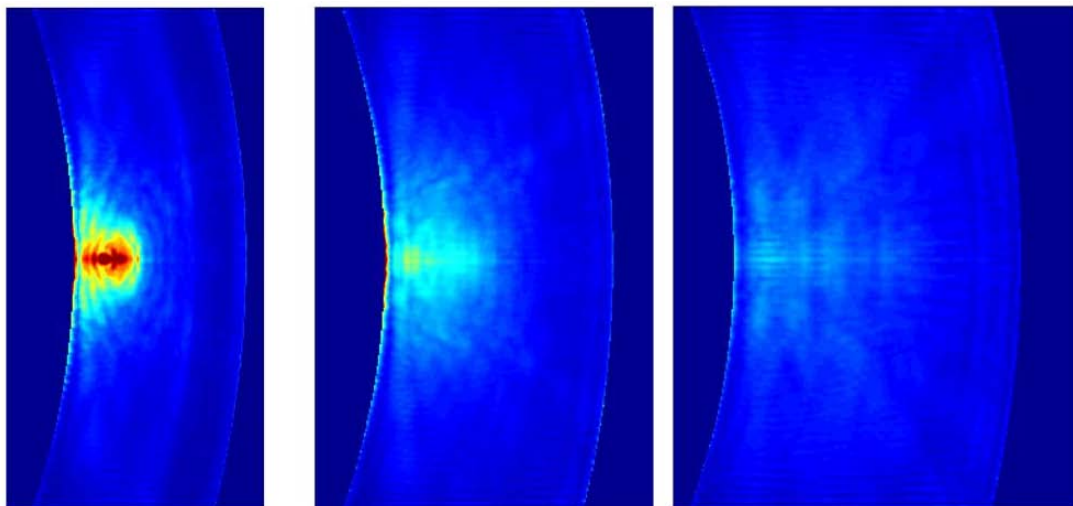


**Fig. (12).** Horizontal slices showing the acoustic energy distribution are shown at shallow, medium, and deep depths into the periodontal anatomy. The curved surface of the tooth is at the left so that the  $z$ -axis of Fig. (6) is now out of the page.

shows the horizontal acoustic energy distribution. Finally, the pressure across the face of the transducer is recorded to create the typical A-line. Fig. (13) shows one of these A-lines indicating the initial burst and two reflections from the internal tip reflections.

## 6. RIGID SIMULATION AND EXPERIMENTAL RESULTS

Systematic rigid simulations were performed to provide an indication of where the echoes from the bottom of the

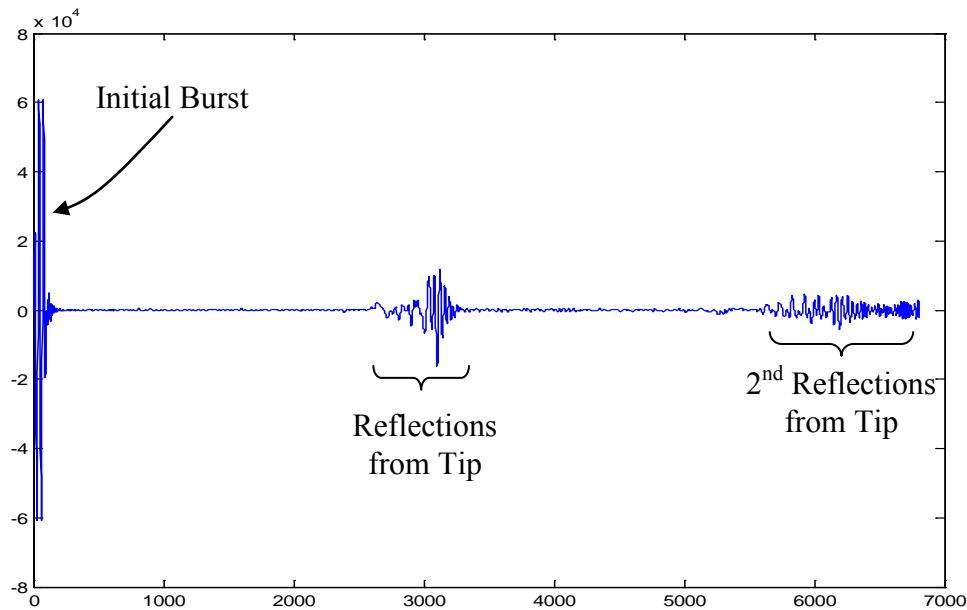


**Fig. (13).** A typical A-line (at 5 MHz) showing the initial burst and two reflections from the tip. The amplitude of the plot is determined by adding the pressure across the tip, and the horizontal axis corresponds to time.

pocket should appear in the A-lines for the realistic simulations. Rigid simulations are performed with the geometry of the periodontal tissues described in the previous sections except that the soft tissues of the gingival and junctional epithelium (JE) are made rigid and hence perfectly reflecting. This guarantees that all of the acoustic energy stays in the water inside the tip and the periodontal pocket and ensures that all the acoustic energy that reaches the bottom of the pocket will be reflected. A total of 40 rigid simulations were performed at 5 MHz with the pocket depth ranging from 0.5 mm to 10.5 mm in 0.25 mm increments. Each of these simulations required about 8 GB of computer memory and took approximately one day to complete when running on 16 computers with CPU speeds of 750 Mhz.

Experimentally, data was collected with an aluminum block with a sequence of holes drilled at different depths, which is a standard test phantom in periodontal probing [52]. The tip and the holes are filled with water just as the periodontal pocket is filled with water in the simulations. The large acoustic impedance mismatch between aluminum and the water keeps almost all of the acoustic energy in the water. Fig. (14) shows A-lines from simulation of the rigid periodontal region and experimental A-lines from the aluminum block at five different depths: 3 mm to 7 mm in 1 mm increments. In both cases, the A-lines have been low-pass filtered and the amplitude of the experimental A-line at 3 mm was reduced to make the plot more consistent since this echo had a very large amplitude. In both the simulated and experimental data peaks are visible and they shift to the right (i.e. later in time) as the depth of the pocket/hole gets deeper.

The differences in amplitudes can be attributed to several experimental and geometrical differences. The experimental data was collected at 10 MHz and includes hardware ampli-

fication. Also, the crevice (or slit like) geometry of the 3D periodontal pocket confines the acoustic energy to two-dimensions while the hole of the experiment confines the energy to one dimension. This would cause the echoes from the experiments to be larger than seen in the simulations.

The velocity of sound in water is approximately  $1482 \text{ ms}^{-1}$ . In the simulated data, the average time between each peak is  $1.334 \mu\text{s}$ . This corresponds to a distance of 2.0 mm or indicating the average depth change of the pocket is 1.0 mm. This distance is indeed the change in pocket depth in between each of the simulations. In the experimental data, the average time between the peaks is  $1.563 \mu\text{s}$  which corresponds to an average change in the depth of the hole of 1.2 mm. This example illustrates that the acoustic simulations of the 3D periodontal pocket can accurately create A-line data with echoes from the bottom of the periodontal pocket that accurately represent the depth of the periodontal pocket. In the more realistic simulations and experimental data, a more sophisticated signal processing technique will be needed to detect the faint echoes from the bottom of the periodontal pocket.

### 7. P ERIODONTAL T ISSUE MA TERIAL PARAME-TERS

Accurate material parameters are necessary to simulate realistic acoustic propagation in the soft tissues surrounding the periodontal pocket. For the 3D acoustic simulations, the material parameters that are needed are the density  $\rho$  and the acoustic wave velocity  $c$ . Unfortunately, we have been unable to find any references that quote these material parameters directly. In previous work, 2D simulations were performed of the tip and the tissue region surrounding the periodontal pocket [48] where the junctional epithelium and gingiva are modeled as skin and muscle, respectively. These

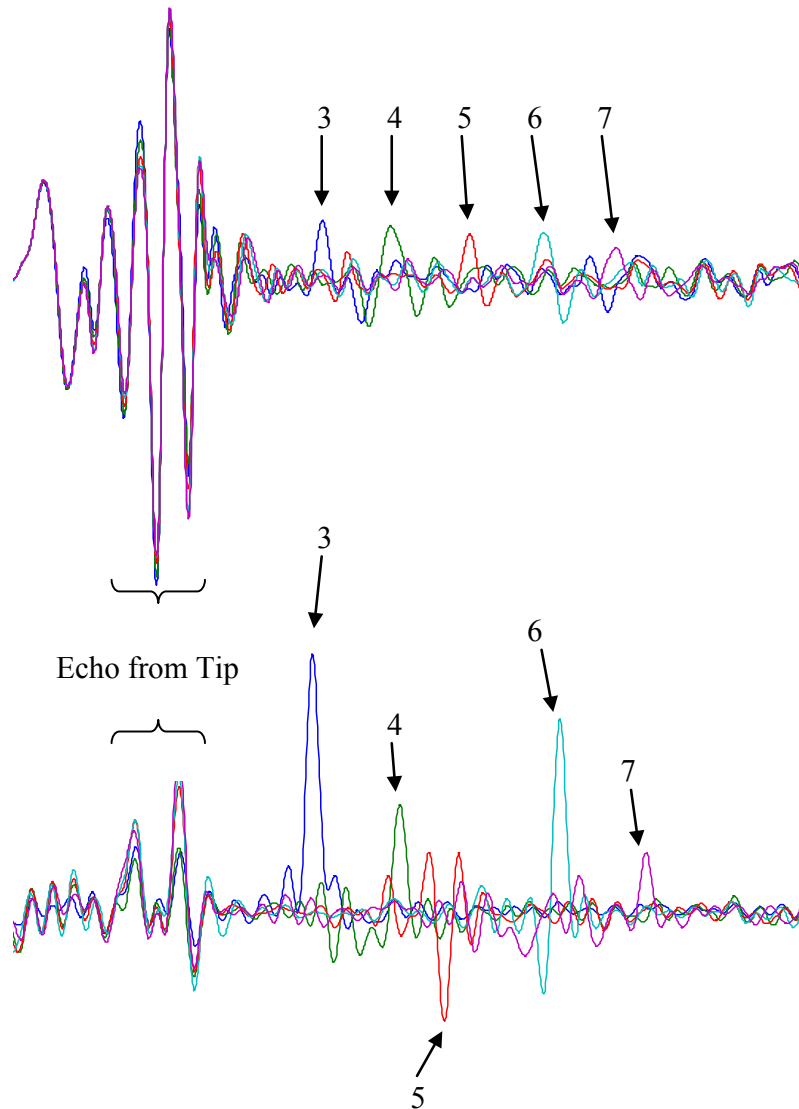


**Fig. (14).** A-lines are plotted for five simulations (top) and five experiments (bottom). The horizontal axis corresponds to time.

values were chosen after extensive discussions with clinical collaborators with expertise in periodontics. We will take the same approach in our 3D simulations.

There are several references for the acoustic material properties of muscle and skin. From [60, 61], we find the density of skin and muscle as  $1020 \text{ kg m}^{-3}$  and  $1080 \text{ kg m}^{-3}$ , respectively. In addition, Culjat *et al.* cite the density and acoustic wave velocity of soft tissue as  $1540 \text{ m s}^{-1}$  and  $1060 \text{ kg m}^{-3}$  [62] and Duck cites the acoustic velocity and density of muscle as  $1550 \text{ m s}^{-1}$  and  $1060 \text{ kg m}^{-3}$  [63]. Table 1 indicates the material parameters used in the 3D simulations. For reference, the acoustic wave velocity and density of water is also presented [64]. These values are close but not exact, and the tissue surrounding the periodontal pocket contains many muscle-like fibers that run perpendicular to acoustic wave propagation direction. This could raise the acoustic impedance mismatch between the water and tissue, so in most

simulations, the acoustic impedance mismatch was increased to account for this fact.

**Table 1. Material Property Values for Soft Tissue Simulation Approximation**

Material	Density Ac	oustic Wave
	( $\text{kg m}^{-3}$ )	Velocity ( $\text{m s}^{-1}$ )
Skin (JE)	1020	1540
Muscle (Gingival)	1080	1550
Water	998.2	1482.1

### 8. 10 MHZ ULTRASOUND BEAM

Describing the 3D ultrasound beam inside the probe tip and the complex tissue structures requires a very sophisti-

cated 3D model. The ultrasound beam is defined by the spatial distribution and intensity of the acoustic energy inside the tissues. The ultrasound beam is difficult to characterize because the beam interacts with several tissue layers in an inherently 3D geometry. Understanding the shape of the ultrasound beam inside the tissues can assist in the interpretation of the experimental A-line measurements.

We use several visualization methods to describe the ultrasound beam inside the tissues. The first is a series of 2D vertical pressure snapshots showing the wave propagation through the probe tip and into the periodontal tissues. Fig. (15) shows several snapshots from a 10 MHz simulation with a pocket depth of 3 mm. These snapshots show that a large portion of the acoustic wave energy is channeled down

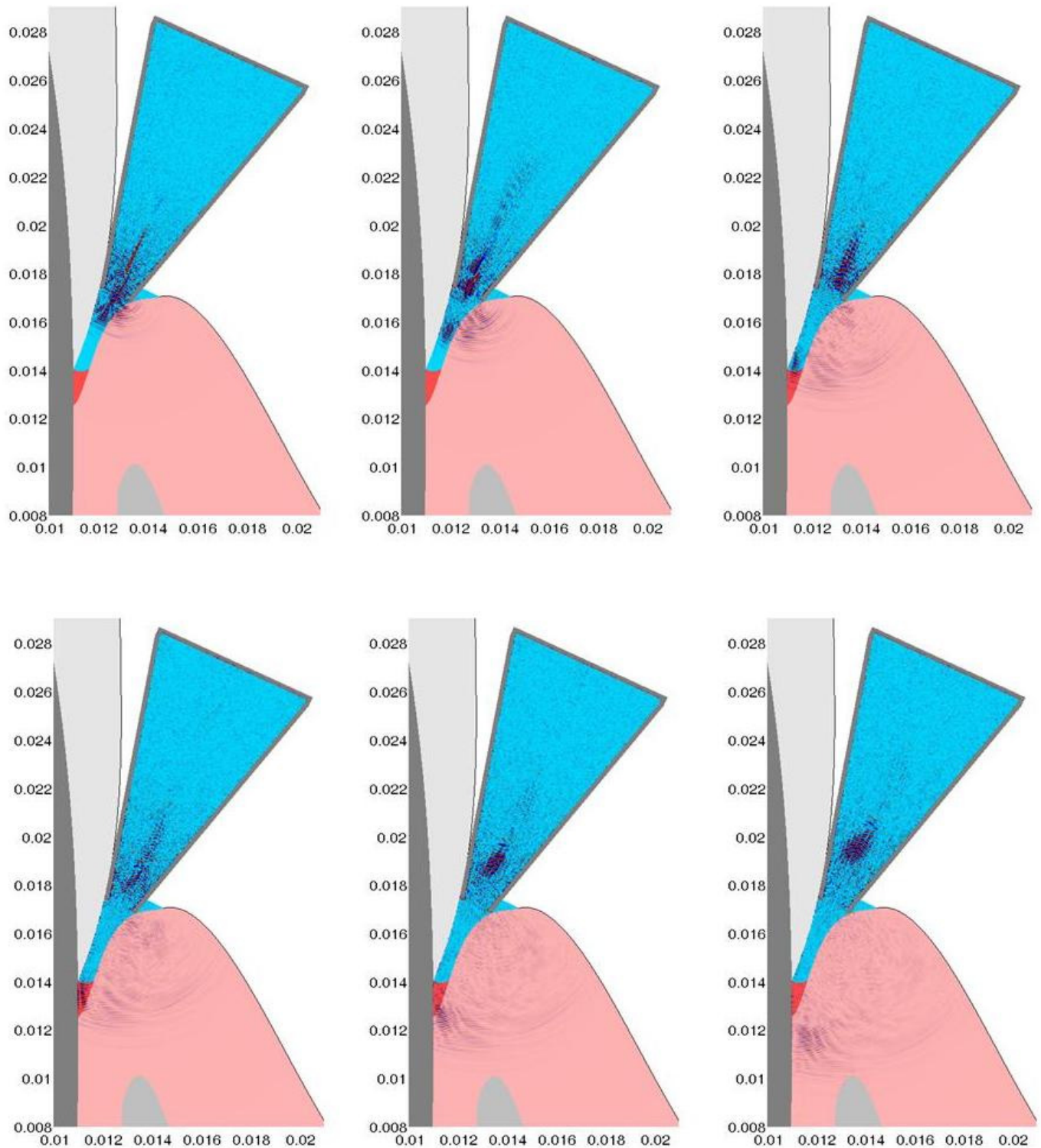
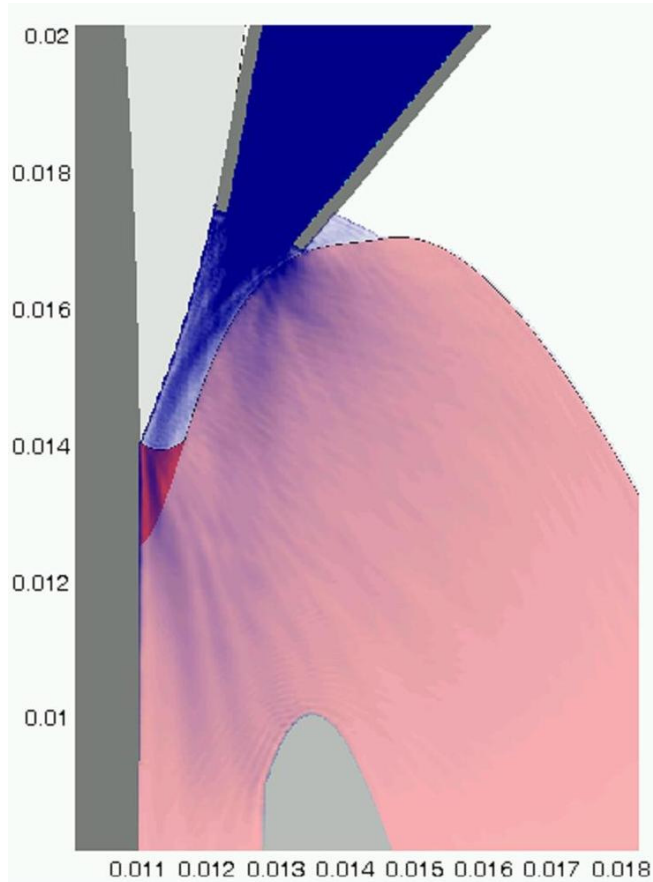


Fig. (15). A series of vertical pressure snapshots showing the acoustic wave progression. In the top center snapshot, the 10 MHz acoustic waves are mostly confined to the pocket or near the interface between the water in the pocket and the gingival tissue.

the water inside the pocket. After the interaction with the bottom of the pocket, the waves scatter off the dentin below the crest and the beam begins to slowly diverge away from the tooth.

Fig. (16) shows a vertical pressure accumulated snapshot where the dark color indicates the spatial distribution of the acoustic energy. This plot also shows a large amount of the acoustic energy is confined to the pocket and scatters off the dentin below the crest. The degree of the scattering off the dentin depends on the angle of the probe tip and the geometry of the tooth structure.



**Fig. (16).** Vertical beam profile from a 10 Mhz simulation showing the spatial distribution of the acoustic energy. The darkness of the blue is proportional to the acoustic energy intensity.

In addition to vertical profile of the ultrasound beam, we also examine horizontal profile slices showing the lateral spread of the beam as it propagates down through the tissue, which gives an indication of the lateral resolution of the device. Fig. (17) contains 12 horizontal beam profile slices located in 0.5 mm increments below the bottom edge of the tip. The colors of the images are proportional to the spatial energy intensity with red being more intense than blue. The right side of these images would correspond to the facial side of the tissue geometry.

In this simulation, the depth of the pocket is 3 mm. In between 0.5 mm and 2.5 mm, one can make out the bound-

ary between the water in the pocket and the soft gingival tissue. As the energy propagates through the tissue, several side lobes form inside the gingival tissue and inside the pocket. The side lobes inside the gingival tissue quickly lose their strength as compared to the main beam inside the pocket. Two side lobes form on either side of the main beam inside the pocket. It is not expected that any measureable returns would come from these side lobes since these lobes diverge away from the main lobe as the waves propagate, and hence any echoes wouldn't be directed back towards the narrow tip orifice. When the acoustic waves interact with the bottom of the pocket (3 mm) the beam is very narrow and close to the tooth surface. From approximately 4 - 6 mm, the beam reflects off the dentin and begins to slowly spread out but the beam is still relatively narrow.

## 9. ENERGY ANALYSIS

In soft tissue versions of the simulation as well as in clinical measurements, the amplitude of the reflections from the periodontal anatomy is on the order of the surrounding noise so that measuring periodontal pocket depth requires sophisticated mathematic techniques. An obvious concern is that not enough of the energy is reaching the anatomy of interest, and so simulations can be used to determine about how much of the energy emitted by the transducer propagates into the periodontal pocket and the junctional epithelium.

As mentioned above, one of the outputs of the simulation is the set of values of the pressure waves in 3D and corresponds to the energy distribution throughout the space. First, the points corresponding to the tissue zone of interest are calculated by finding the outline of the tissue zone in the 2D simulation and rotating those points in a manner similar to the rotation technique of the original simulation to fill the tissue zone in 3D. Next, for each cross-sectional depth, we can find the energy in the tissue zone at that depth by using the following formula:

$$\dot{E} = I \cdot da = \sum_{grid} \frac{p^2}{\rho c} A \approx \sum p^2 \quad (1)$$

In Equation 1, energy ( $\dot{E}$ ) flux is related to the intensity ( $I$ ) over an area element ( $da$ ) by the above equation. The acoustic energy of a plane wave is directly related to the square of the pressure ( $p$ ) divided by density times acoustic speed of sound ( $c$ ) [65]. In our case, these last two quantities are similar enough for all the regions of interest, being close to that of water, and will drop out due to normalization. Therefore, in the simulation, the 3D pressure values correspond to the energy by the sum of the square of the pressure values at each point in the tissue zone. Rather than averaging over time, discrete values of time were chosen because of constraints on the simulation run time. Three zones of interest were selected: the junctional epithelium, where the manual periodontal probe is thought to bottom out, as well as the gingiva and the water in the periodontal pocket.

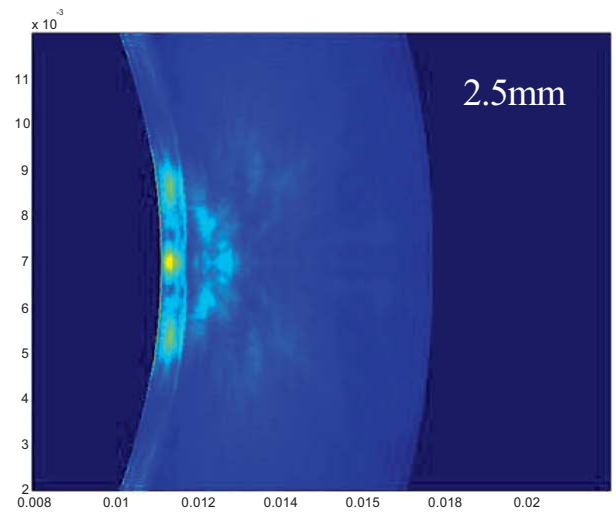
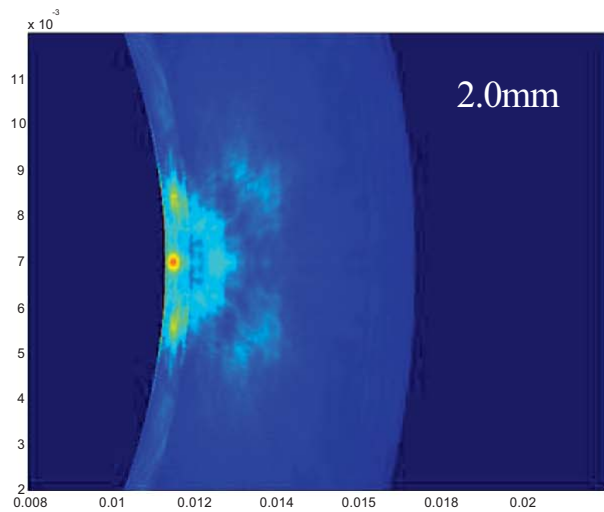
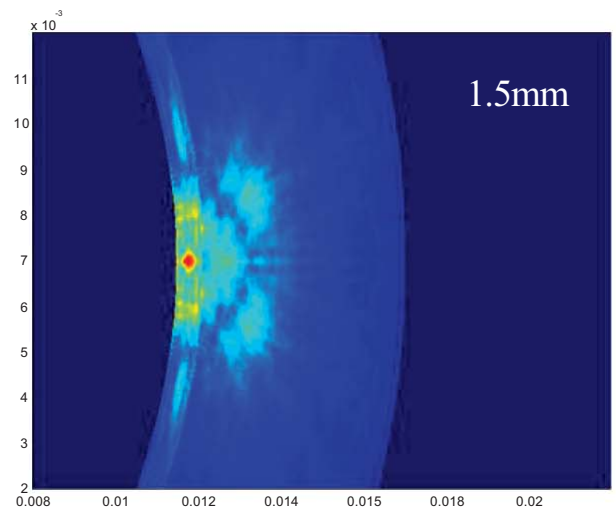
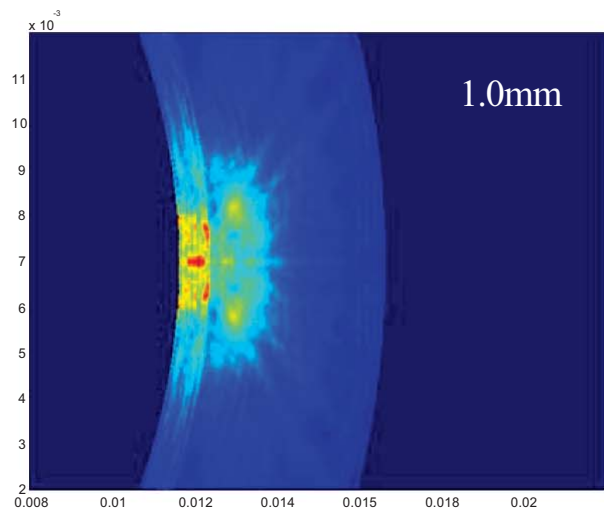
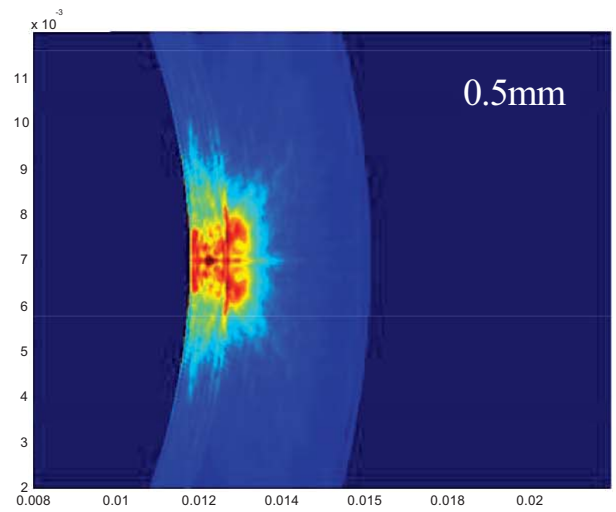
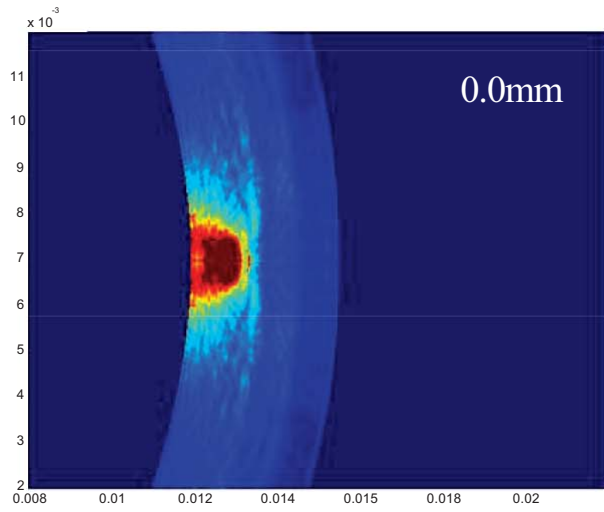


(Fig. 17) contd.....

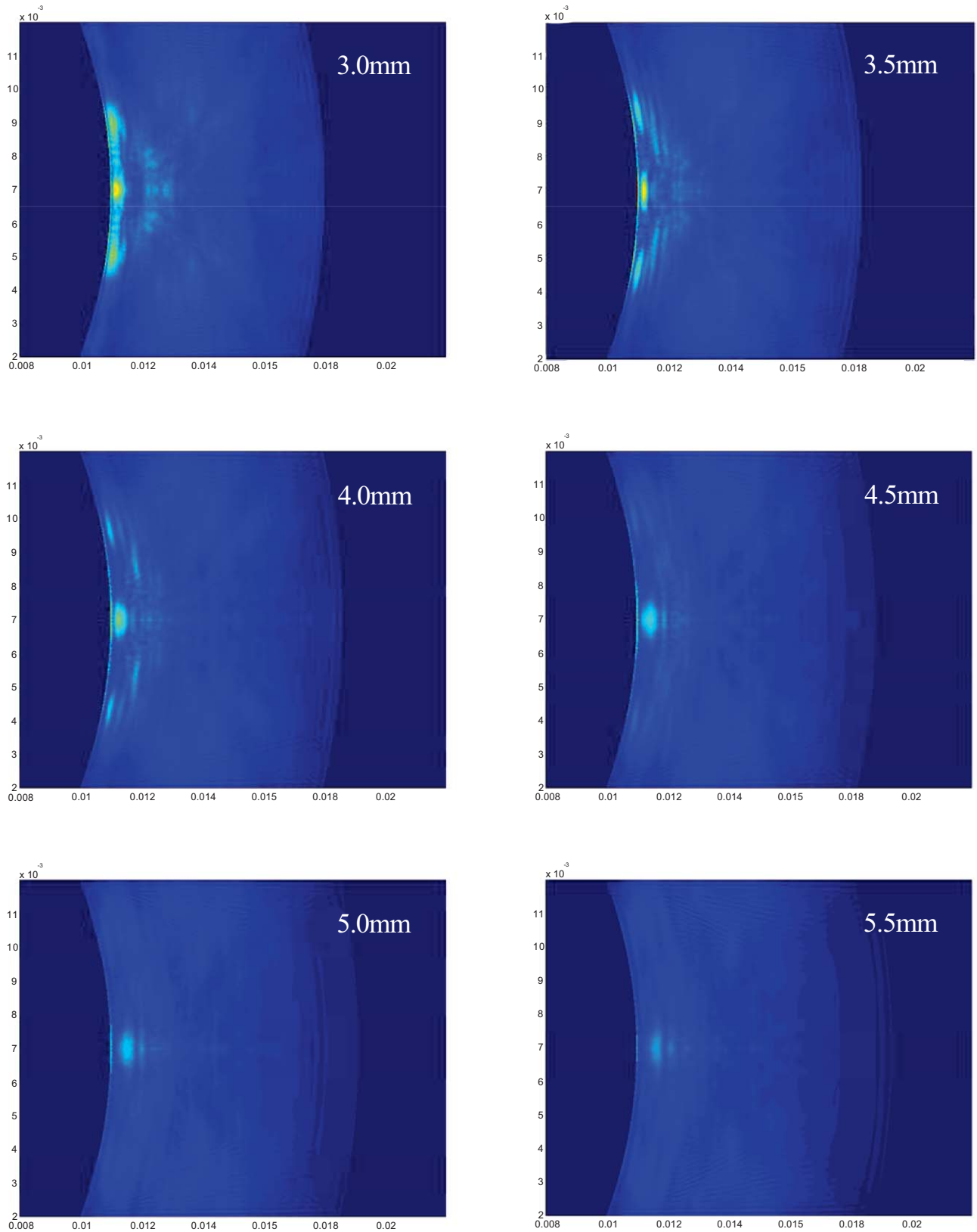


**Fig. (17).** A series of horizontal beam profiles showing the lateral resolution of the ultrasound beam at 10 MHz.

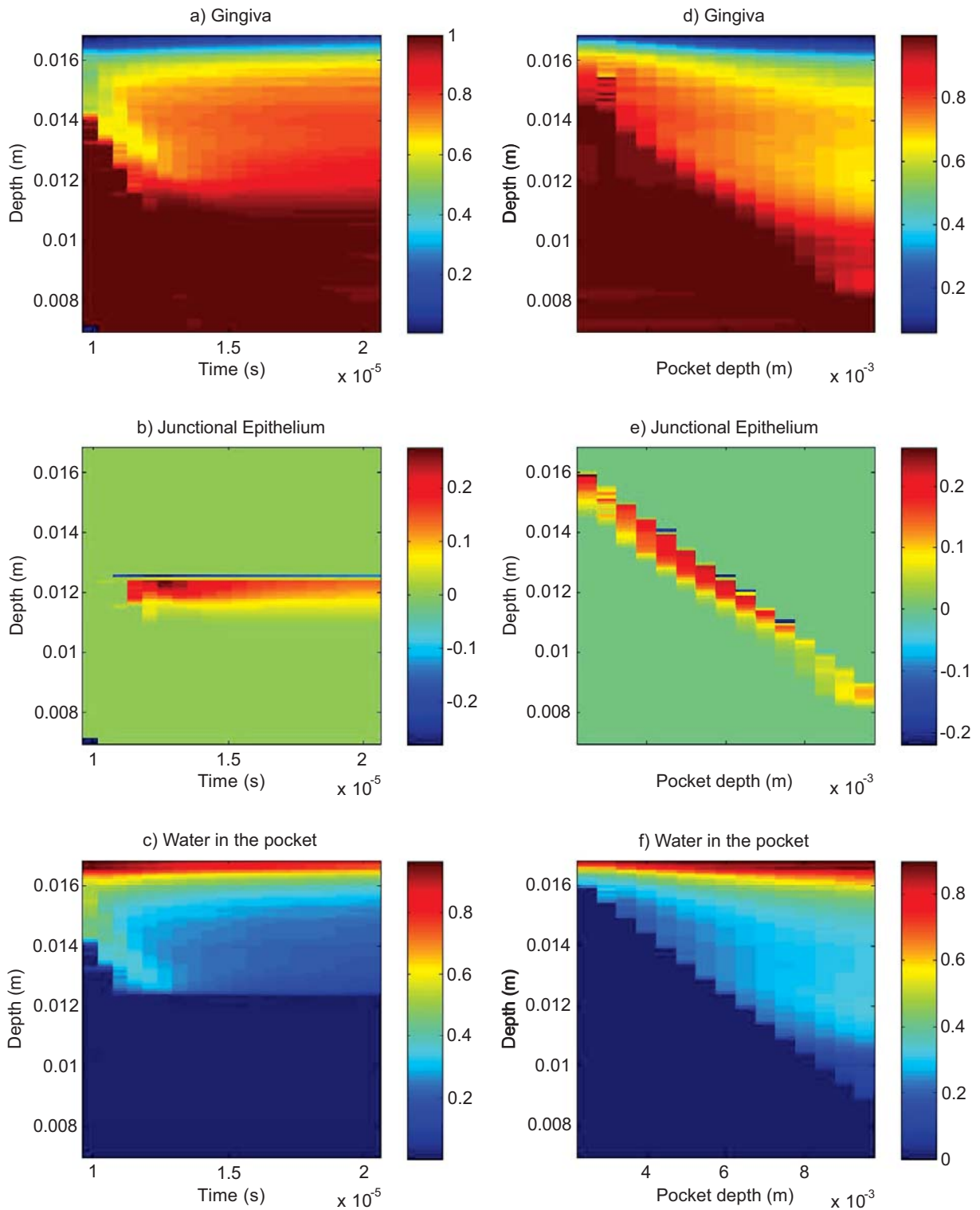


**Fig. (18).** Energy values of the soft tissue approximation are displayed in a phase space. The  $z$ -axis of the physical simulation space (Fig. 6) is the same as the vertical of these phase space plots. The horizontal axis in these phase space plots correspond to the independent variable of the simulation, either time in the simulation or energies of different pocket depths. (a-c) are simulations in which pocket depth is held constant while pressure values were captured at varying times in the simulation, while (d-f) are simulations in which pressure values are captured at only one time but pocket depth varies. The color bar legend on the right of each graph indicates amplitude of the resulting energy ratio normalized by energy available at the indicated height in the anatomy.

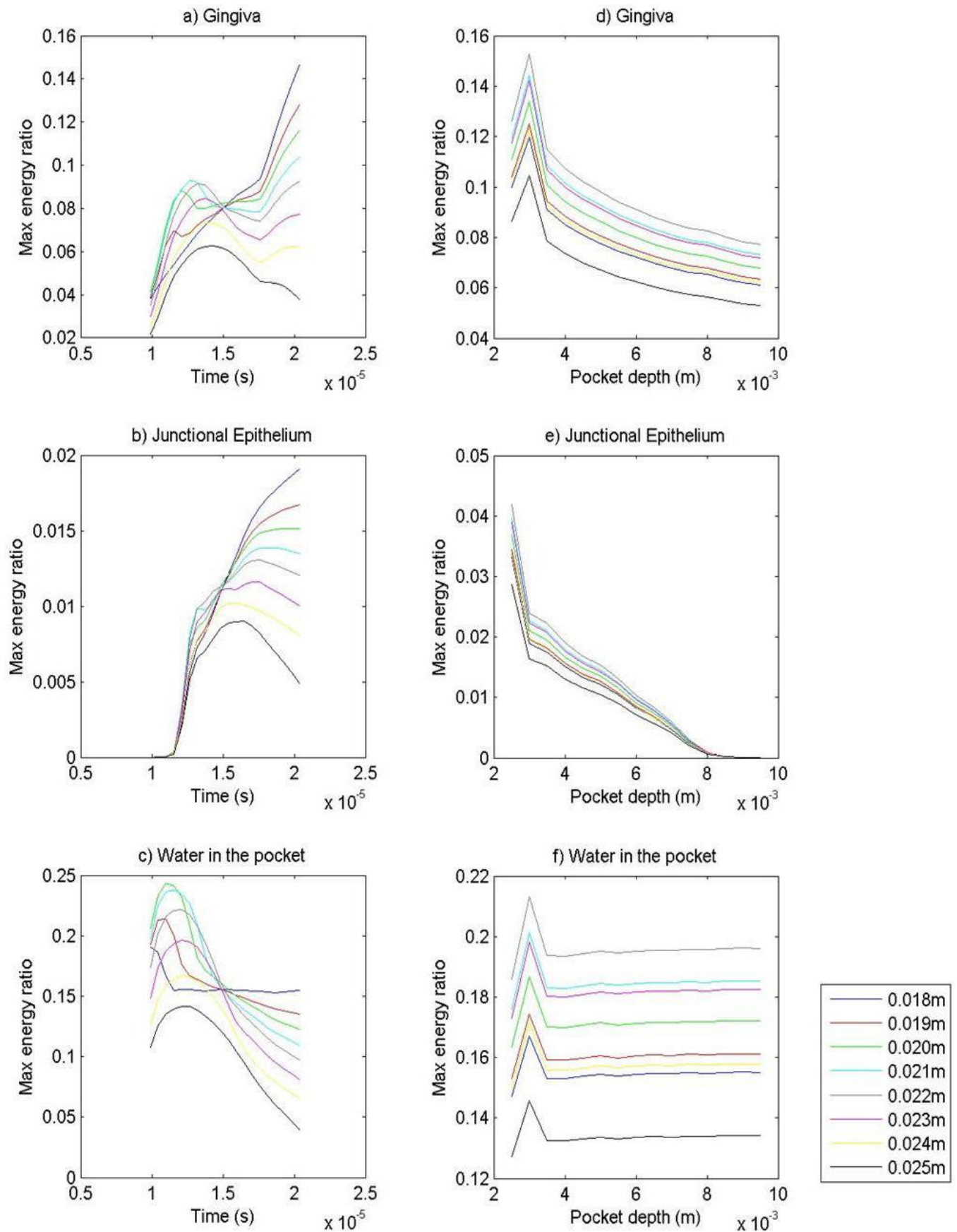


**Fig. (19).** The energy values are now normalized by energies at 8 different points in the tip, and the maximum of the energy was selected and plotted against the dependent variable of the simulation.

Simulations were performed with soft tissue approximation as described in Table 1 using a 10 MHz transducer. The energy values were normalized two different ways: first, the energy values in each tissue zone were normalized with respect to the total energy values at that depth, and second, the total energy in the tip at 8 different depths was used. Because of internal reflections and constructive/destructive interference within the tip, the energy in the tip is not constant. At any point in the simulation, interference of reflections in the tip may seem to cause more energy in different regions than in others, and so 8 different points in the tip were chosen for normalization. Also, two different types of simulations were performed. In the first, one pocket depth was chosen (0.060 m from the bottom of the junctional epithelium, which is 1.5 mm thick) and pressure values were recorded for 20 different time intervals. In the second, the pocket depth was varied from 0.025-0.095 m and the pressure values were recorded at one time snapshot corresponding to 1.37e-5 s in the simulation. In the simulation geometry, the origin of the anatomy occurs toward the root of the tooth, so that large values of anatomy height (up to 0.300 m) correspond to regions closer to the transducer part of the tip, while low values of anatomy height correspond to regions below the pocket. For all of the energy studies, the maximum anatomy height displayed corresponds to the point where the tip meets the anatomy, while the lowest anatomy height displayed corresponds to points well below the junctional epithelium. See Fig. (6) for the relative periodontal anatomy in the simulation.

Fig. (18) shows the energy ratio in the three different regions normalized by energy available at that height for simulations varying by time or pocket depth. As expected, the gingiva holds the largest percentage of the available energy, as it does take up most of the space. The water in the pocket holds the next largest available energy, which is located mostly closest to where the tip meets the anatomy. The most energy in the junctional epithelium is located earlier in space and time, which makes sense, since the energy has the least opportunity to be diffused. When normalized relative to the energy available at that height, there is at most 27.6% of the energy collected in the junctional epithelium, which is considerable.

Fig. (19) shows the max energy ratio in the zones of interest normalized by the energy in different points of the tip. The energy ratio results for the gingiva are illuminating, because at best, 15.3% of the energy in the tip is translated into the anatomy at all. In all cases, the largest energy ratio results when the zone's energy is normalized with respect to the point in the tip closest to the anatomy. It is also encouraging that as much as 24.3% of the energy in the tip propagates to the water in the pocket. However, very little of the energy in the tip propagates to the junctional epithelium, less than 4%. This is a manifestation of the fact that no sizable reflection from the junctional epithelium is visible in the soft tissue approximation simulation A-lines. Table 2 gives a numerical summary of these results.

In all, little of the energy present in the tip propagates to the junctional epithelium, a reflection from which would correspond to the manual periodontal probe measurement.

Hence, standard peak location measurements will not be sufficient to translate the ultrasonographic probe measurements to manual probe measurements but sophisticated mathematical techniques may be able to resolve the 4% of the energy present in the junctional epithelium.

10. CONCLUSIONS

We have developed a three-dimensional parallel acoustic finite integration technique to simulate acoustic wave propagation in the complex geometry of the periodontal anatomy. A set of software tools automatically creates the 3D geometry of the periodontal region and runs systematic simulations. Several techniques are used to visualize the ultrasound waves inside the tip and in the periodontal pocket and surrounding tissues.

Rigid simulations were performed to show that the simulation software can produce realistic data with echoes corresponding to the depth of the periodontal pocket. A set of 10 MHz simulations were completed to describe the ultrasound beam inside the tissue. In addition many systematic simulations were performed to create a large data set to assist in the development of the signal processing algorithms to automatically detect the pocket depth. Energy studies indicate, as expected, that between 1-4% of the energy in the tip propagates to the junctional epithelium, so that no large reflections from that region can be expected to show in the resulting waveform. These simulations confirm observed experimental data from our ultrasonographic periodontal probe. Future work will focus on developing signal processing techniques to detect the faint echoes from the bottom of the periodontal pocket, which is the key remaining technical challenge to making ultrasonographic probing useful for measuring periodontal pocket depth.

Table 2. Maximum Energy Values (%)

	Normalized by Total Energy			Normalized by Tip Energy		
	Gingiva	JE P	ocket	Gingiva	JE P	ocket
Time Varies	1.000	0.276	0.967	0.146	0.019	0.243
Pocket Depth Varies	1.000	0.262	0.899	0.153	0.042	0.213

The maximum values of energy values for each of the three zones are displayed here for both types of normalizations and both simulations. In the case of those normalized by tip energy, the maximum value of the energy ratio over the 8 different tip locations was selected.

ACKNOWLEDGEMENTS

Partial support for this work was provided by the Virginia Space Grant Consortium. The authors would also like to thank Chris Bording for his assistance with parallel computing on SciClone.

REFERENCES

[1] Loesche WJ, Grossman NS. Periodontal disease as a specific, albeit chronic, infection: diagnosis and treatment. Clin Microbiol Rev 2001; 14(4): 727-52.

- [2] Socransky SS, Haffajee AD, Smith C, Dibart S. Relation of counts of microbial species to clinical status at the sampled site. *J Clin Periodontol* 1991; 17: 788-92.
- [3] Evans CA, Kleinman DV. The surgeon general's report on America's oral health: opportunities for the dental profession. *J Am Dent Assoc* 2000; 131(12): 1721-8.
- [4] Barrington EP, Nevins M. Diagnosing periodontal diseases. *J Am Dental Assoc* 1990; 121(4): 460-4.
- [5] Armitage GC. Diagnosis of periodontal diseases. *J Periodontol* 2003; 74: 1237-47.
- [6] Albandar JM, Brunelle JA, Kingman A. Destructive periodontal disease in adults 30 years of age and older in the United States, 1988-1994. *J Periodontol* 1999; 70(1): 13-29.
- [7] Oliver RC, Brown LJ, Loe H. Periodontal diseases in the United States population. *J Periodontol* 1998; 69(2): 269-78.
- [8] Papapanou PN. Periodontal diseases: epidemiology. *Ann Periodontol* 1996; 1(1): 1-36.
- [9] Fowler EB. Periodontal disease and its association with systemic disease. *Mil Med* 2001; 166: 85-9.
- [10] Paquette DW. The periodontal infection-systemic disease link: a review of the truth or myth. *J Int Acad Periodontol* 2002; 4: 101-9.
- [11] Slots J. Update on general health risk of periodontal disease. *Int Dent J* 2003; 53: 200-7.
- [12] Beck JD, Pankrow J, Tyroler HA, Offenbacher S. Dental infections and atherosclerosis. *Am Heart J* 1999; 138: S528-S533.
- [13] Loesche WJ, Schork A, Terpenning MS, Chen Y-M, Dominguez BL, Grossman N. Assessing the relationship between dental disease and coronary heart disease in elderly U.S. veterans. *J Am Dent Assoc* 1998; 129(3): 301-11.
- [14] Mattila KJ, Valtonen VV, Nieminen MS, Asikainen S. Role of infection as a risk factor for atherosclerosis, myocardial infarction, and stroke. *Clin Infect Dis* 1998; 26: 719-34.
- [15] Trovato JP. The role of the general dentist in periodontal care. *Gen Dent* 2003; 51(2): 176-81.
- [16] Haffajee AD, Socransky SS, Goodson JM. Clinical parameters as predictors of destructive periodontal disease activity. *J Clin Periodontol* 1982; 10: 257.
- [17] Rams TE, Slots J. Comparison of two pressure-sensitive periodontal probes and a manual probe in shallow and deep pockets. *Int J Periodontics Restorative Dent* 1993; 13: 521-9.
- [18] Lang NP, Corbet EF. Diagnostic procedures in daily practice. *Int Dent J* 1995; 45: 5-15.
- [19] Greenstein G, Lamster I. Understanding diagnostic testing for periodontal diseases. *J Periodontol* 1995; 66: 659-66.
- [20] Listgarten MA. Periodontal probing: What does it mean? *J Clin Periodontol* 1980; 7: 165-76.
- [21] Hunter F. Periodontal probes and probing. *Int Dent J* 1994; 44: 557-83.
- [22] Mayfield L, Bratthall G, Attström R. Periodontal probe precision using 4 different periodontal probes. *J Clin Periodontol* 1996; 23: 76-82.
- [23] Tupta-Veselicky L, Famili P, Ceravolo FJ, Zullo T. A clinical study of an electronic constant force periodontal probe. *J Periodontol* 1994; 65: 616-22.
- [24] Cattabriga M. Future diagnostic possibilities in periodontology. *Int Dent J* 1993; 43: 109-15.
- [25] Yang MCK, Marks RG, Magnusson I, Clouser B, Clark WB. Reproducibility of an electronic probe in relative attachment level measurements. *J Clin Periodontol* 1992; 19: 306-11.
- [26] Ahmed N, Watts TLP, Wilson RF. An investigation of the validity of attachment level measurements with an automated periodontal probe. *J Clin Periodontol* 1996; 23: 452-5.
- [27] Aguero A, Garnick JJ, Keagle J, Steflik DE, Thompson WO. Histological location of a standardized periodontal probe in man. *J Periodontol* 1995; 66: 184-90.
- [28] Keagle JG, Garnick JJ, Searle JR, Thompson WO. Effect of gingival wall on resistance to probing forces. *J Clin Periodontol* 1995; 22: 953-7.
- [29] Ghorayeb SR, Bertoncini CA, Hinders MK. Ultrasonography in Dentistry. *IEEE Trans Ultrason Ferroelectr Freq Control* 2008; 55(6): 1256-66.
- [30] Spranger H. Ultra-sonic diagnosis of marginal periodontal diseases. *Int Dent J* 1971; 21(4): 442-55.
- [31] Muraoka Y, Sueda T, Kinoshita S. Examination of periodontal tissue with an ultrasonic apparatus. Measurements of the thickness of gingiva, alveolar mucosa and alveolar bone. *Nippon Shishubyo Gakkai Kaishi* 1982; 24(4): 601-6.
- [32] Sawada K, Fujimasa T, Sunada I. Ultrasonography of the periodontal tissue. *Nippon Shishubyo Gakkai Kaishi* 1984; 26(1): 88-93.
- [33] Lost C, Nussle W. Periodontal ultrasonic diagnosis: experiments on thin bony platelets and on a simulated periodontal ligament space. *J Periodontol Res* 1988; 41(9): 347-51.
- [34] Palou ME, McQuade MJ, Rossmann JA. The use of ultrasound for the determination of periodontal bone morphology. *J Periodontol* 1987; 58(4): 262-5.
- [35] Walmsley AD, Laird WR, Lumley PJ. Ultrasound in dentistry. Part 2 - Periodontology and endodontics. *J Dent* 1992; 20(1): 11-7.
- [36] Ohshima K. Application of ultrasonography to periodontal diagnosis. *Nippon Shishubyo Gakkai Kaishi* 1989; 1: 235-40.
- [37] Eger T, Müller H-P, Heinecke A. Ultrasonic determination of gingival thickness. *J Clin Periodontol* 1996; 23(9): 839.
- [38] Tsiolis FI, Needleman IG, Griffiths CS. Periodontal ultrasonography. *J Clin Periodontol* 2003; 30: 849-54.
- [39] Loker DR, Hagenbuch K. Ultrasonic periodontal diagnostic instrumentation system with clinical results. *Measurement* 1998; 23(3): 125-9.
- [40] Demyun SM, Hagenbuch KM. Ultrasonic method and apparatus for measuring the periodontal pocket. US Patent 5,100,318, March 31, 1992.
- [41] Hinders M, Companion J. Ultrasonic Periodontal Probe. In: Thompson DO, Chimenti DE, Eds. 25th Review of Progress in Quantitative Nondestructive Evaluation; July 1998; New York, Plenum Press, 1998; vol. 18b: pp. 1609-15.
- [42] Hinders MK, Guan A, Companion J. Ultrasonic periodontal probe. *J Acoust Soc Am* 1998; 104(3): 1844.
- [43] Hartman SK. Goodbye Gingivitis. Virginia Business, 1997: 9.
- [44] Companion JA. Differential measurement periodontal structures mapping system. US Patent 5,755,571, May 26, 1998.
- [45] Farr C. Ultrasonic probing: The wave of the future in dentistry. *Dent Today* 2000; 19: 86-91.
- [46] Hinders MK, Lynch JE, McCombs GB. Clinical tests of an ultrasonic periodontal probe. In: Thompson DO, Chimenti DE, Eds. 28th Review of Progress in Quantitative Nondestructive Evaluation; August 2001; Melville, New York: AIP Conference Proceedings, 2001; vol. 21b: pp. 1880-90.
- [47] Lynch JE, McCombs GB, Hinders MK. Periodontal disease diagnosis using a non-invasive sonographic probe: Advancements in Ultrasonic Symposium; Alexandria, VA. 9 May 2001.
- [48] Lynch JE. Ultrasonographic measurement of periodontal attachment levels. PhD [dissertation]. Williamsburg (VA): College of William and Mary 2001.
- [49] Lynch JE, Hinders MK. Ultrasonic device for measuring periodontal attachment levels. *Rev Sci Instrum* 2002; 73(7): 2686-93.
- [50] Hou JR. Ultrasonic signal detection and characterization using dynamic wavelet fingerprints. PhD [dissertation]. Williamsburg (VA): College of William and Mar 2004.
- [51] Hinders MK, Hou JR. Ultrasonic periodontal probing based on the dynamic wavelet fingerprint. In: Thompson DO, Chimenti DE, Eds. 31<sup>st</sup> Review of Progress in Quantitative Nondestructive Evaluation; July 2004; Melville, New York, AIP Conference Proceedings 2004; vol. 24b: pp. 1549-56.
- [52] Hou JR, Rose ST, Hinders MK. Ultrasonic periodontal probing based on the dynamic wavelet fingerprint. *EURASIP J Appl Signal Process* 2005; 7: 1137-46.
- [53] Lynch JE, Hinders MK, McCombs GB. Clinical comparison of an ultrasonographic periodontal probe to manual and controlled-force probing. *Measurement* 2006; 39(5): 429-39.
- [54] Hinders MK, McCombs GB. The Potential of the Ultrasonic Probe. *Dimens Dent Hyg* 2006; 4(4): 16-8.
- [55] Hou J, Hinders MK. Dynamic Wavelet Fingerprint identification of ultrasound signals. *Mater Eval* 2002; 60(9): 1089-93.
- [56] Schoen DH, Dean M-C. Contemporary periodontal instrumentation. WB Saunders: Philadelphia 1996.
- [57] Wilkins EM, Ed. Clinical practice of the dental hygienist. Lippincott Williams & Wilkins: Philadelphia 2005.
- [58] Carranza FA, Newman MG, Eds. Clinical periodontology. WB Saunders: Philadelphia 1990.
- [59] Rateitschak KH, Rateitschak EM, Wolf HF, Hassell TM. Periodontology. In: Rateitschak, KH, Ed. Color Atlas of Dental Medicine, Thieme Medical Publishers, New York 1989.

- [60] Madsen EL, Sathoff HJ, Zagzebski JA. Ultrasonic shear wave properties of soft tissues and tissuelike materials. *J Acoust Soc Am* 1983; 74: 1346-55.
- [61] Goss SA, Johnston RL, Dunn F. Comprehensive compilation of empirical ultrasonic properties of mammalian tissues. *J Acoust Soc Am* 1978; 64: 423-56.
- [62] Culjat MO, Singh RS, Brown ER, Neurgaonkar RR, Yoon DC, White SN. Ultrasound crack detection in a simulated tooth. *Dentomaxillofac Radiol* 2005; 34: 80-5.
- [63] Duck FA. Physical properties of tissue. Academic Press: London 1990.
- [64] Kinsler L, Frey AR, Coopens AB, Sanders J. Fundamentals of acoustics, 4<sup>th</sup> ed. John Wiley & Sons, Inc: New York 2000.
- [65] Morse PM, Ingard KU. Theoretical acoustics. Princeton University Press: Princeton, NJ 1968.

---

Received: September 30, 2008

Revised: November 7, 2008

Accepted: November 19, 2008

© Rudd *et al.*; Licensee *Bentham Open*.

This is an open access article licensed under the terms of the Creative Commons Attribution Non-Commercial License (<http://creativecommons.org/licenses/by-nc/3.0/>) which permits unrestricted, non-commercial use, distribution and reproduction in any medium, provided the work is properly cited.